water

MDPI

Article

Lake Evolution, Hydrodynamic Outburst Flood Modeling and Sensitivity Analysis in the Central Himalaya: A Case Study

Ashim Sattar [1,*], Ajanta Goswami [1], Anil. V. Kulkarni [2] and Adam Emmer [3]

1 Indian Institute of Technology, Roorkee 247667, India; ajantagoswami@gmail.com
2 Indian Institute of Science, Bangalore 560012, India; anilkulkarni@iisc.ac.in
3 The Czech Academy of Sciences, Global Change Research Institute, 603 00 Brno; Czech Republic; aemmer@seznam.cz
* Correspondence: ashim.sattar@gmail.com; Tel.: +91-9557289744

Received: 14 November 2019; Accepted: 10 January 2020; Published: 15 January 2020

Abstract: Climate change has led to the formation of numerous high-altitude lakes of glacial origin in the Himalaya. Safed Lake is one of the largest glacial lakes, located at an elevation 4882 m a.s.l. in the state of Uttarakhand, central Himalaya, India. A temporal analysis of the lake surface using satellite imagery shows that the lake has grown more than double its size from 0.10 km^2 to 0.23 km^2 over the past 50 years. In this study, we performed a hazard assessment of the lake using 1D and 2D hydrodynamic modeling. We identified the potential glacial lake outburst flood (GLOF) triggering factors and evaluated the impact of a moraine breach event of the lake on the nearest village located 16.2 km downstream of the lake. A series of dynamic simulations were performed for different scenario-models based on varied breach depths, breach widths and time of moraine failure. In a worst-case GLOF scenario where breach depth reached up to 60 m, hydrodynamic routing of the breach hydrograph along the given channel revealed inundation depth up to 5 m and flow velocities up to 3.2 m s^{-1} at Milam village. Considering the flat geometry of the frontal moraine, hazard assessment of the lake was performed by for different breach incision depths (30 and 15 m). In addition, the study incorporated a series of hydrodynamic routing to understand the sensitivity of GLOF to different model input parameters and terrain conditions. The sensitivity of the initial GLOF hydrograph to breach formation time (T_f) was evaluated by considering different hypothetical breach scenarios with a varied time of failure. Increases of 11.5% and 22% in the peak flooding were recorded when the moraine failure time was decreased by 15 and 30 min respectively. The two-dimensional sensitivity revealed flow velocity (m s^{-1}) to be more sensitive to change in Manning's N when compared to the inundation depth (m). Changes of 10.7% and 0.5% in the mean flow velocity (in m s^{-1}) and flow depth (in m) were recorded when dN was 0.01. The flow velocity was more sensitive to the slope and the top-width of the channel when compared to the inundation depths. A regression of flow velocity versus slope gives a correlation coefficient of 0.76. GLOF flow hydraulics are sensitive to changes in terrain elevation, where flow depth and velocity vary in a similar manner.

Keywords: GLOF; HEC-RAS; hazard assessment; hydrodynamic modeling; Indian Himalaya; Uttarakhand

1. Introduction

Facing climate change-induced decline of glaciers associated with the formation and evolution of glacial lakes in the Hindu Kush-Karakoram-Himalaya (HKKH) region (e.g., [1,2]), glacial lake

outburst floods (GLOFs) are considered an emerging threat [3]. Despite the fact that the overall number of documented GLOFs has been recently doubled by employing an advanced remotely sensed image-based approach, the frequency of GLOFs is apparently unchanged since the 1980s [4], that being explained by the lagged response of glaciers and lakes in the region [5]. Regardless of that fact, research on GLOFs in the HKKH attracted increased scientific attention in past years [6], and 2013 Kedarnath disaster with a death toll of 6000 [7] highlighted the need for GLOF risk assessment and management. Particularly in India, GLOFs were shown to cause significant damage [8].

Previous lake and GLOF studies in the Indian Himalaya were performed on different scales, ranging from nationwide lake inventories and GLOF assessments to detailed case studies focusing on individual lakes. The nationwide lake inventory and GLOF risk assessment were done by Worni et al. [9], identifying 251 lakes, of which 104 were considered potentially dangerous or dangerous; state-wide assessments were done, e.g., by Allen et al. [10] for Himachal Pradesh, and by Raj et al. [11] and Aggarwal et al. [12] for Sikkim. Basin-wide assessments were done, e.g., by Shrestha et al. [13] for Nepal, by Jain et al. [14] for a part of the Garwhal basin and by Mir et al. [15] for Zanskar basin. Examples of detailed case studies are the work of Sharma et al. [16] and Sattar et al. [17], both focusing on South Lhonak Lake (Sikkim). Considering the amount of potentially dangerous lakes identified from various region-wide assessments, studies evaluating GLOF hazard of individual lakes and GLOF modeling studies are still quite rare, despite the need for such studies being well-recognized in disaster management plans (DMPs) of individual mountain states of India [18].

In this particular case study, we focused on detailed assessment of the evolution and potential GLOF hazard of Safed Lake located in Uttarakhand, Central Himalaya, with special attention paid to the sensitivity assessment of hydrodynamic model used. Specific objectives of this study were: (i) to document the evolution of Safed Lake in time, using remotely sensed images going back to 1968; (ii) to model a potential worst-case GLOF scenario, using HEC-RAS 1D and 2D, and to identify exposed elements in the nearest settlement (Milam village located 16.2 km downstream); and (iii) to evaluate the sensitivity of the HEC-RAS hydrodynamic model to changes in input parameters (Manning's N, breach width (B_w), breach formation time (T_f) and channel characteristics (slope, terrain elevation and top-width). Our work targets the scientific community (by providing detailed insights into the sensitivity of the HEC-RAS model and its potential for being employed in GLOF studies) and disaster risk reduction practitioners (by providing GLOF hazard implications).

2. Study Area

Safed Lake (30°33′46.55′′ N and 80°10′19.15′′ E) is located in the northern part of the Goriganga basin in the state of Uttarakhand, Central Himalaya, India (see Figure 1). The basin is drained by the Goriganga river, originating from the Milam glacier. The lake is located in a hanging valley, and the lake level is at 4882 m a.s.l. It is the largest proglacial lake in the basin with a total area of 0.23 km^2 (in 2018) and underwent significant glacier retreat-induced growth in past decades (see Section 4.1). The lake is dammed by a relatively flat moraine-periglacial debris complex with a "hummocky" surface, suggesting the possible presence of buried ice cores. As such, the dam is considered susceptible to failure. At the same time, the lake is surrounded by several steep slopes, which are potential sources of mass movements into the lake. The cliff located in the left bank of the lake is very steep, with slopes varying between 35° and 70° (see Figure 2a). Also, being a proglacial lake, it is located at the snout of the parent glacier, which is marked by a tall ice-wall and a zone of glacier-calving (see Figure 2b). The upper part of the valley is not permanently inhabited; however, Milam village (30°26′03.82′′ N and 80°09′03.04′′ E) is located 16.2 km downstream of the lake at the confluence of the Gonka and Gori rivers with an elevation of 3419 m.a.s.l. Milam is a small village in the Pithoragarh district with a population of only 135. It consists of a total of 110 buildings spread over an area of 0.25 km^2.

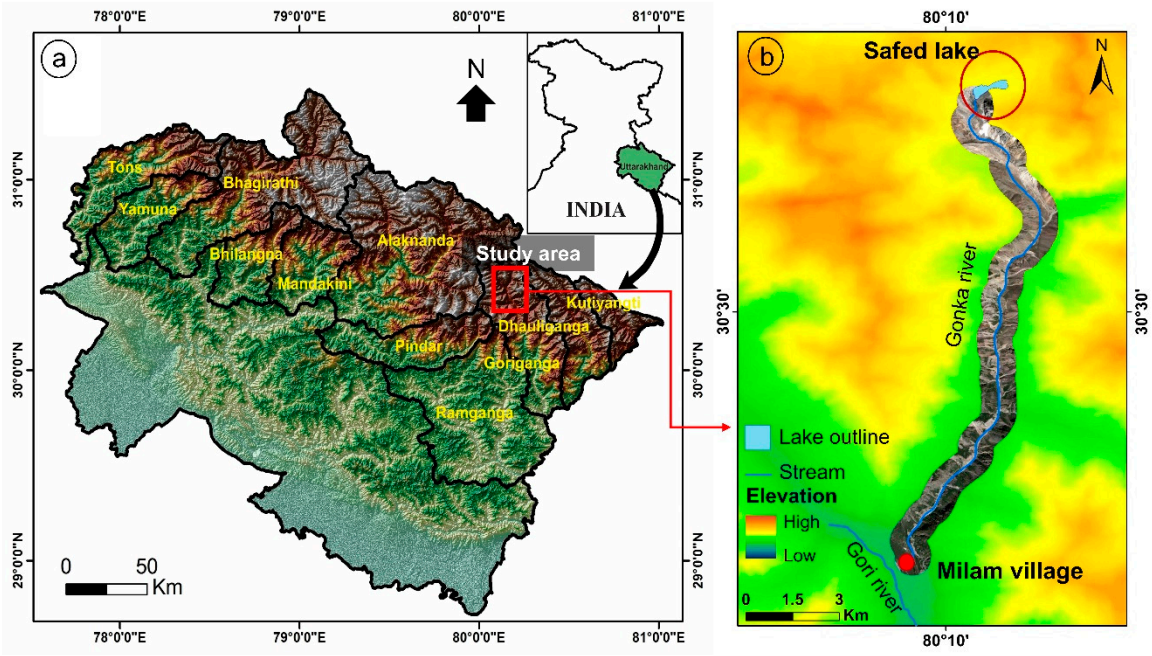

Figure 1. (**a**) The state of Uttarakhand and the location of the study area in the Goriganga basin; (**b**) the location of Safed Lake and Milam village; the village is located at the confluence of the Gorka and the Gori rivers.

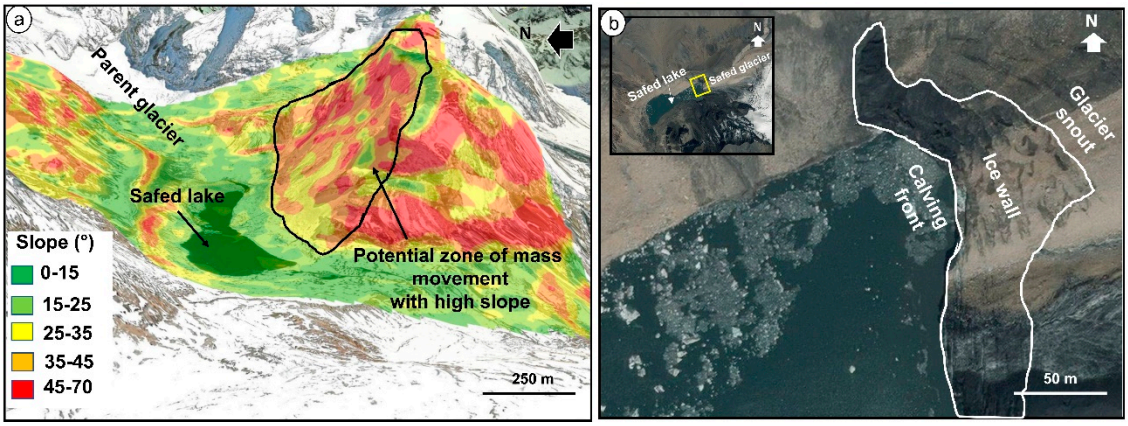

Figure 2. (**a**) The source zone of potential mass movements; (**b**) calving zone at the snout of the glacier. All images: Google Earth [19].

3. Data and Methods

3.1. Remotely Sensed Data and the Growth Assessment of Safed Lake

A growth assessment of Safed Lake was performed using multitemporal satellite images. We used Corona (KH4) (5.6 m), Landsat TM, Landsat ETM+ and OLI/TIRS (30 m) to map the lake's extent from 1968 to 2018 (years 1968, 1994, 2000 and 2018). The images used in the study were selected during the end of a hydrological year, towards the end of September to avoid seasonal or inter-annual variation. Terrain data for GLOF modeling was obtained from Advanced Spaceborne Thermal Emission and Reflectance Radiometer (ASTER) global digital elevation model (GDEM; version 2). ASTER Digital Elevation Model (DEM) is a freely available model (https://earthexplorer.usgs.gov/) that provides elevation information between 83° N and 83° S with a spatial resolution of 30 m and vertical accuracy of ≈10–20 m for hilly terrains [20,21]. ASTER GDEM has certain limitations related to the spatial resolution; e.g., underestimation of the valley floor elevations [22]. It is, however, the best freely available DEM for the remote Indian Himalaya. The land use land cover (LULC) classification,

to determine Manning's roughness coefficient (Manning's N) of the given terrain, was obtained using GlobCover (version 2) and cross-verified using high-resolution geo-referenced CNES/Airbus imagery tiles of Google Earth [19]. GlobCover is the global product of land cover maps created from the 300 m MERIS sensor onboard of the ENVISAT satellite [23].

The normalized difference water index (NDWI) [24] was employed to identify and map the lake's surface area. In order to check the accuracy of mapping, the lake's outlines were overlapped on high-resolution Google Earth imageries using GIS-based tools. The orthorectification of the historical image (Corona) has been carried out using ground control points (GCP). The Corona subset image of the lake with no cloud cover and minimum snow was used to calculate the total area for the year 1968. Further, we employed the rubber sheeting method to orthorectify the given image using a total of 50–70 GCP's from high-resolution geo-referenced CNES/Airbus imagery tiles [19], which reduced the uncertainty significantly to less than a pixel (in the total area calculations). The lake boundaries were delineated manually using the rectified Corona images. Corona images had previously been used successfully for mapping the glaciated terrain in Himalaya [11,25,26]. Since the present study aimed to evaluate the GLOF hazard of Safed Lake at a present scenario, we considered the latest extent (2018) of the lake for volume estimation and flood routing.

3.2. Hazard Assessment of Safed Lake

Due to the absence of bathymetric data for Safed Lake, we employed an area-based scaling relationship to calculate the total volume of the lake. Several empirical relationships are available to roughly estimate the total volume of glacial lakes based on the total surface area [24,27–31]. The relation given by Huggel et al. [24] is among the most widely used and has been employed in several previous GLOF hazard studies, where no direct bathymetric measurements are available [14,32–37]. The total water volume was calculated considering the total surface area in 2018. The equation [24] is given as:

$$V = 0.104\, A^{1.42} \tag{1}$$

where V is the total volume of the lake and A is the area of the lake. The total volume of the lake was calculated to be 4.34×10^6 m^3. A difference of 7% (higher) was calculated when compared to the volume estimates obtained from the Huggel et al. [24] equation in the total lake volume using the equation of Cook and Quincey [27] ($V = 0.1217\, A^{1.4129}$). Despite this is a rough estimate, we considered this volume estimation for the modeling of the worst-case GLOF scenario for Safed Lake. Apart from that, we also considered releases of 50% and 25% of the total lake volume (see below).

One-dimensional modeling (HEC-RAS) was employed to calculate the breach hydrograph. The average breach width and failure time were calculated using the empirical relations given by Froehlich [38]:

$$B_w = 0.1803 K_o \times (V_w)^{0.32} \times (h_b)^{0.19} \tag{2}$$

$$T_f = 0.00254 \times (V_w)^{0.53} \times (h_b)^{-0.9} \tag{3}$$

where B_w is the breach width (in m), V_w is the volume of the lake (in m^3), h_b is the height of the breach (in m) and T_f (in h) is the time taken for the breach to form (where distances B_w and h_b are fully reached; see Figure 3). Here, the volume calculated using Equation (1) is considered to derive the breach parameters. The h_b is derived from DEM and is considered to be 60 m, assuming that the moraine breaches up its base, in a worst-case scenario. Based on the above equations, the breach width Equation (1) and breach formation time Equation (2) in a worst-case scenario are calculated to be 73.13 m and 0.21 h respectively (Scenario 1; Table 1).

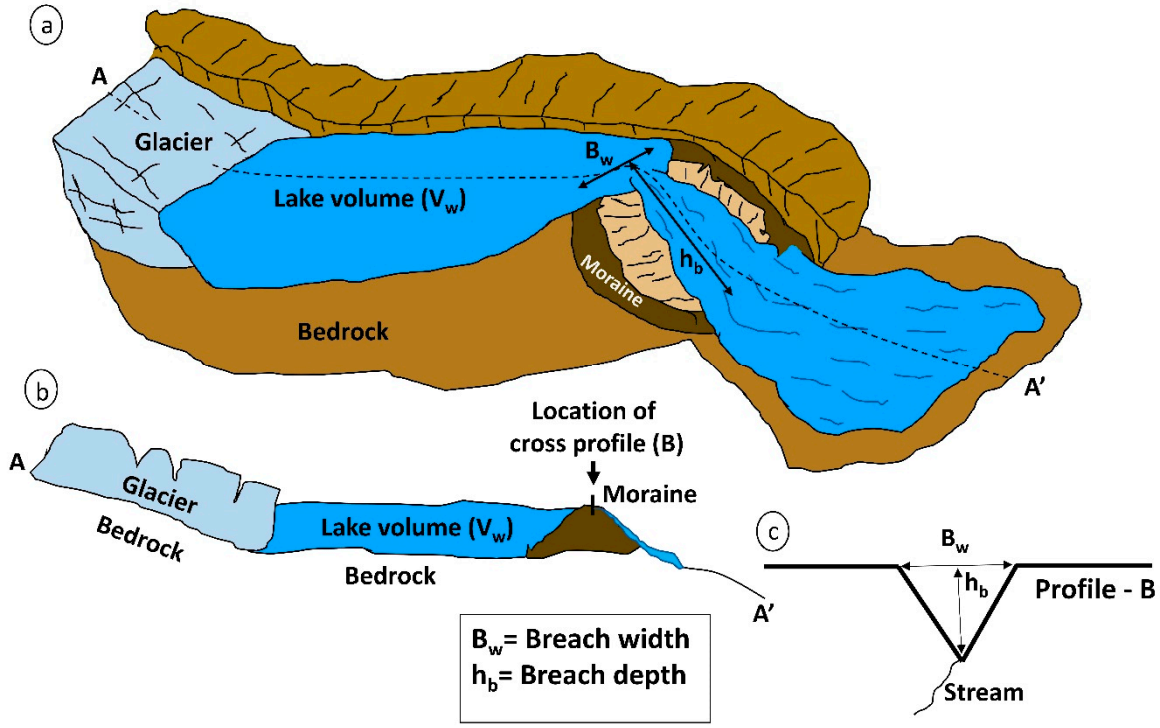

Figure 3. Schematic showing (**a**) a moraine-dammed glacial lake showing breach width (*Bw*) and breach depth (h_b); (**b**) valley longitudinal profile along AA'; (**c**) moraine dam post-failure cross profile (see (**b**) for location).

Table 1. Breach parameters for scenario modeling calculated based on Froehlich (1995).

GLOF Scenarios	Breach Depth (h_b)	Volume Released (in m^3)	Percentage Lake Volume Released	Breach Width (B_w) (in m)	Time of Failure (T_f) (in h)
Scenario 1	60	4.34×10^6	100	73.13	0.21
Scenario 2	30	2.17×10^6	50	51.33	0.27
Scenario 3	15	1.08×10^6	25	35.97	0.34

However, considering the flat geometry of the dam (a relatively large width of >400 m, and a distal face of the dam with a slope <25%, which is comparatively gentle compared to the maximum slope which moraine dams can reach), it is unlikely that the moraine incision would take place up to a depth of 60 m. Therefore, apart from the worst-case scenario, we considered two different scenarios based on varied breach depth (h_b) (30 and 15 m) and total volume of water released in a potential GLOF event (Scenarios 2 and 3; Table 1). Assuming that the volume released in a potential GLOF event of Safed Lake varies linearly with the breach depth, we constructed the model in a way that half of the total volume and quarter of the total volume were released for breach depth of 30 and 15 m respectively (Scenarios 2 and 3). These GLOF scenarios allowed us to capture the wide variability of diverse GLOF triggers and their magnitudes, which we hoped would lead us to different process chains. The breach parameters for all the given models were calculated based on Froehlich [38] m and are given in Table 1. The time of failure (T_f) is an inverse function of the breach depth (h_b), and therefore, it is longer for shallower depth [38].

The HEC-RAS 1D model [39] was employed to model a series of potential GLOF events of Safed Lake. Despite that this tool has not been widely employed in Uttarakhand previously, it has been successfully employed in GLOF modeling (both reconstructing past GLOFs and modeling potential future GLOFs) in different geographical settings and contexts (e.g., [40–42]). As such, we were convinced this tool would provide physically plausible modeling results in our case too.

The initial breach hydrograph was constructed for each scenario based on the parameters given in Table 1. The worst-case GLOF scenario of the lake is revealed in Scenario 1 (B_w = 73.13 m and T_f = 0.21 h). Two-dimensional hydraulic routing of the breach hydrographs calculated for Scenario 1, Scenario 2 and Scenario 3 was performed for a distance of 16.2 km from the lake up to Milam village to evaluate its impact on the village. The HEC-RAS 2D (version 5.0.5; Brunner [43]) was used to rout the initial breach hydrographs along the main flow channel. The primary input of the model includes terrain data and boundary conditions for simulating an unsteady hydraulic process. ASTER DEM raster was used as a continuous terrain input. A flow area was initially defined over the given terrain, containing the area of interest; i.e., the lake to Milam village. A 2D mesh was constructed within the given flow area, with an individual cell dimension of 30 × 30 m. The land use/land cover (LULC) for the flow area was extracted from GlobCover [23]. Further, a value of Manning roughness was defined to each cell based on the LULC. An average Manning's N within the flow area was calculated to be 0.05, which was considered for routing. Spatially distributed hydraulic properties (flow velocity and inundation depth) were mapped along the channel for a distance of 16.2 km from the lake to the village.

3.3. Sensitivity Analysis

3.3.1. Model Sensitivity to Input Parameters

A series of hydraulic simulations were performed to evaluate the sensitivity of the hydrodynamic model to the input parameters (Manning's N and breach parameters). Here, we assess the sensitivity of the model to the dam-breach parameters (breach width and breach formation time) in order to evaluate its effect on the initial breach hydrograph. A total of six hypothetical one-dimensional moraine breach simulations were performed with varied breach width (B_w) and time of failure (T_f). Three scenarios with T_f = 0.50 h, T_f = 0.75 h and T_f = 1.0 h with a constant B_w =100 m were considered to evaluate the sensitivity of the model to T_f. Similarly, keeping T_f constant, the model sensitivity to B_w was evaluated by considering three scenarios with varied B_w (50, 75 and 100 m). The peak discharge and time of peak in each scenario were compared to assess the sensitivity of the model to the input parameters. Moreover, to evaluate the two-dimensional sensitivity of the model to the above hypothetical breach hydrographs, the modeled hydrographs were routed along the flow channel from the lake to Milam village. A Manning's N of 0.05 was considered for dynamic routing (Section 3.3.2). The model sensitivity was evaluated by assessing the change in the flow hydraulics (inundation depth and flow velocity) for the different upstream boundary conditions (input hydrographs).

In order to evaluate the sensitivity of the model to Manning's N, a series of two-dimensional routings of the dam-breach hydrograph (obtained in a worst-case scenario, Scenario 1) was performed. This was achieved by the two-dimensional routing of the potential moraine-breach hydrograph for varied Manning's N (0.03, 0.04, 0.05, 0.06 and 0.07). The model sensitivity was evaluated by assessing the change in the flow depth and flow velocity (maximum and mean) for different values of Manning's N.

3.3.2. Sensitivity to Channel Characteristics and DEM Used

The sensitivity of the flow hydraulics of a modeled potential GLOF (Section 4.2) to the slope and top-width of the channel (GLOF inundation width) was evaluated. The slope was calculated for each 100 m elevation interval along the entire length of the given flow channel (from the lake to Milam village). The mean velocity in each 100 m elevation band was calculated from the obtained spatially-distributed 2D modeled results and plotted against its respective slope values to evaluate its relationship. Similarly, the modeled 2D flow depth was extracted for every elevation band, and the mean depth calculated for each band was plotted against the slope of the channel for the sensitivity evaluation.

The sensitivity of the modeled results to the top-width of the flow channel was evaluated by analyzing the variation in the hydraulic properties for different channel top-width. For this, the width of the modeled GLOF inundation in the given channel was measured across 20 cross-sections. Further,

the top-width (in m) was plotted against the mean flow velocity (ms^{-1}) and inundation depth (m) calculated along the different cross-sections. The variations of flow depth and velocity to the different top-widths of the channel were then evaluated.

Since DEM is a critical element for GLOF route modeling, we evaluated the sensitivity of the GLOF hydraulics to the terrain data (DEM) by comparing the flow hydraulics, performed over two different DEMs (ASTER and SRTM). We considered the worst-case GLOF scenario (Scenario 1; $B_w = 73.13$, $T_f = 0.21$) for flood routing over both ASTER DEM (Section 3.2) and SRTM DEM. We divided the flow channel (3200–4960 m a.s.l.) into elevation bands of 250 m each (7 bands). The terrain elevation values of each DEM (ASTER and SRTM) were extracted within the inundation boundary of each elevation band. The difference in the elevation was calculated using raster-based operations for the elevation bands (SRTM elevation – ASTER elevation). Similarly, we calculated the difference in the routed flow depth (m) and flow velocity (m/s) over each DEM (SRTM flow hydraulics – ASTER flow hydraulics). Further, we plotted the average flow depth difference (in m) and average flow velocity (in m/s) difference against the elevation difference (m) for the given elevation bands.

4. Results

4.1. Growth of Safed Lake

The lake surface for the year 1968 was mapped by visual interpretation of the high-resolution Corona image. The lake grew to more than double its size over a period of 50 years, from 0.10 km^2 in 1968 to 0.23 km^2 in 2018. The total lake-surface areas for the years 1994 and 2000 were measured to be 0.14 km^2 and 0.16 km^2 respectively. Figure 4 shows the growth of Safed Lake in the last five decades. We observed accelerating average annual glacier retreat and associated lake growth over the analyzed period: 1.48×10^3 m^2 per year (1968–1994); 2.86×10^3 m^2 per year (1994–2000); 3.68×10^3 m^2 per year (2000–2018). Since the lake is in its proglacial phase of evolution, future growth is excepted as the glacier continues to retreat.

4.2. Hazard Assessment of Safed Lake

The occurrence of GLOF is controlled by two factors—dam stability and the possibility of a triggering event. As for dam stability, we consider moraine/periglacial debris dam of Safed Lake to be potentially unstable, and moreover possibly filled with buried ice cores (see Section 2); therefore, we consider the dam susceptible to breaching and failure, despite relatively flat geometry. As for the triggers, Safed Lake is located in the close proximity to steep slopes and we found mass movements from these slopes to be the most likely triggers of potential GLOF from this lake.

Froehlich's [23] equations were employed to model a series of potential GLOFs of Safed Lake. In the worst-case scenario (Scenario 1, see Table 1), the breach event was modeled considering a breach width (B_w) of 73.13 m and time of failure (T_f) of 0.21 h. The GLOF hydrograph produced a peak discharge of 8181 m^3s^{-1} that was achieved within 6 min after the initial breach event. Figure 5 shows the breach hydrograph in a worst-case GLOF scenario of Safed Lake. Since we modeled the breach formation in a "Sinewave" progression and not in a "linear" progression, we expected a peak before the breach was fully developed. In addition, two different potential GLOF scenarios were modeled, for which breach parameters were calculated based on varied breach depth (h_b) and the volume of water (m^3) released (see Table 1). In Scenario 2 ($h_b = 30$, $B_w = 51.33$ m, $T_f = 0.27$ h) the GLOF hydrograph releasing the half (1/2) the volume of the lake produced a peak of 5110 m^3 s^{-1} (peak attained in 12 min after the initial breach event). Similarly, a GLOF hydrograph was constructed considering a new set of breach parameters ($h_b = 15$, $B_w = 35.97$ m, $T_f = 0.34$ h), releasing 1/4 of the lake volume (Scenario 3). A peak discharge of 1495 m^3 s^{-1} was attained 22 min after the initial moraine breach event.

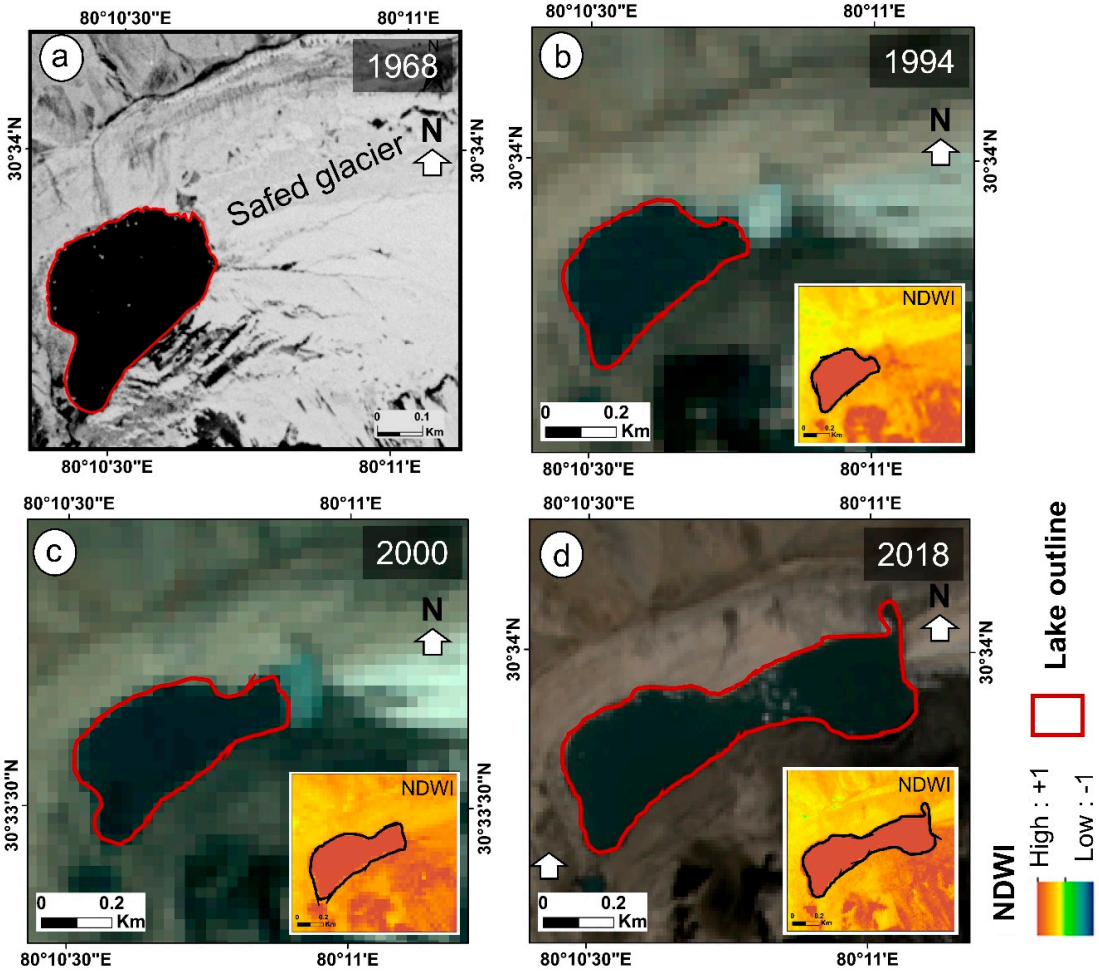

Figure 4. The growth of Safed Lake from 1968 to 2018 (**a**–**d**); the subset image (in **b**–**d**) shows the Normalized Differential Water Index (NDWI) for the respective years.

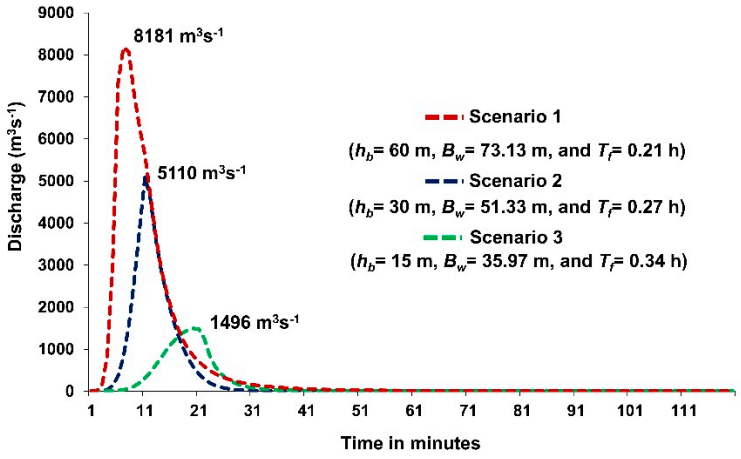

Figure 5. The potential moraine-breach hydrograph of Safed Lake. A peak discharge of 8181 m^3s^{-1} was reached within 6 min after the initiation of the dam breach event (worst-case scenario: Scenario 1); breach hydrographs for varied breach depth (h_b) (30 m and 15 m) and total volume of water released in a potential glacial lake outburst flood (GLOF) event (Scenarios 2 and 3) (see Table 1).

In order to evaluate the potential impact of a Safed Lake GLOF on Milam village, two-dimensional hydraulic routing of the breach hydrographs obtained in Scenario 1 (h_b = 60 m, releasing full lake

volume), Scenario 2 (h_b = 30 m, releasing 1/2 the lake volume) and Scenario 3 (h_b = 15 m, releasing 1/4 of the lake volume) were performed. The assessment of the two-dimensional temporal hydraulics at Milam village in the worst-case scenario (Scenario 1), revealed flow depths up to a maximum of 5.0 m, which was achieved in 1 h 15 min after the initial dam breach event (Figure 6). The flow velocities at the village reach up to 3.2 m s^{-1} and the peak occurs at the same time as the maximum flow depth. The potential GLOF inundates a total area of 0.02 km^2 at Milam village. The GLOF potentially inundates four minor settlements consisting of a total of 25 to 30 buildings. However, the major part of the village remains unaffected by the GLOF as it located at approximately 200 m towards the west. Figure 7 shows the potentially inundated settlements at Milam village, and the plots showing the change of inundation depth and flow velocity with time.

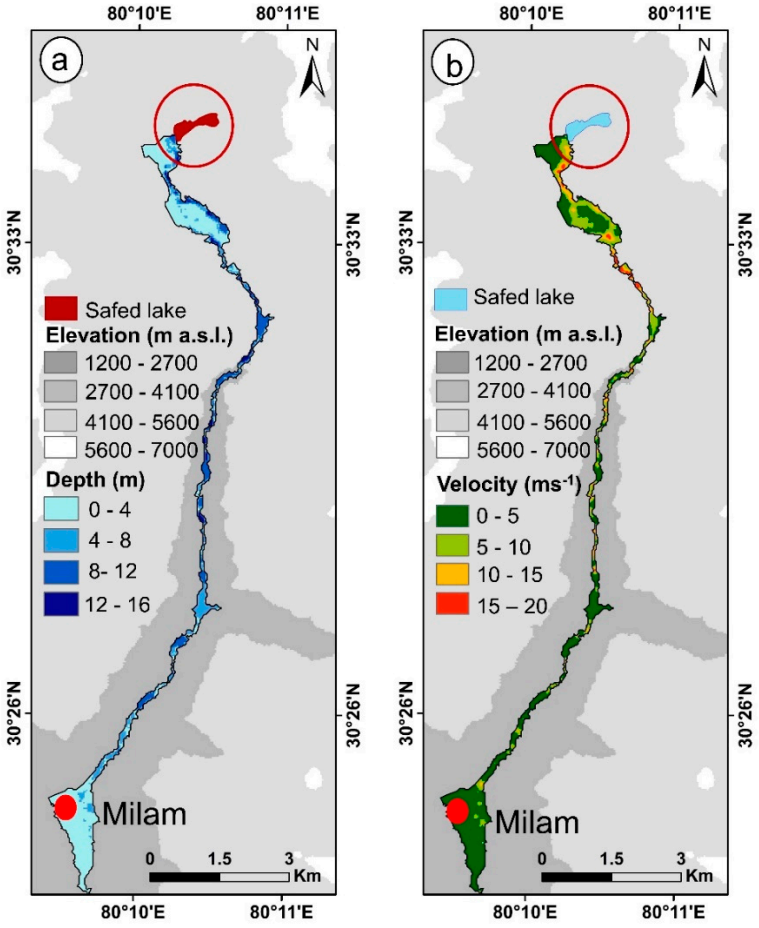

Figure 6. Spatially distributed plots of (**a**) inundation depth (in m) and (**b**) flow velocity (m s^{-1}) along the flow channel in a worst-case scenario from the lake to Milam village (Scenario 1).

In Scenario 2, the maximum inundation depth and flow velocity at Milam village reach up to 2.3 m and 1.3 m s^{-1} respectively. The GLOF arrives in the village at 2 h after the breach event and the peak is reached within 15 min of the flood wave arrival. The total GLOF inundation reduces by 31% when compared to Scenario 1. In Scenario 3, the inundation depth reaches up to a maximum of 0.9 m at Milam village with flow velocities reaching up to 0.3 m s^{-1}. The peak in the flow hydraulics is attained in 6 h 35 min after the initial breach event of Safed Lake. The longer time taken here for the flood to reach Milam village can be attributed to the fact that the GLOF discharge is very low and the bed-resistance dominates the convective acceleration of the flow. The total inundation is reduced by 63% when compared to the worst-case scenario (Scenario 1). Table 2 summarizes the hydraulics of the GLOF hydrographs and the routed flow properties at Milam village.

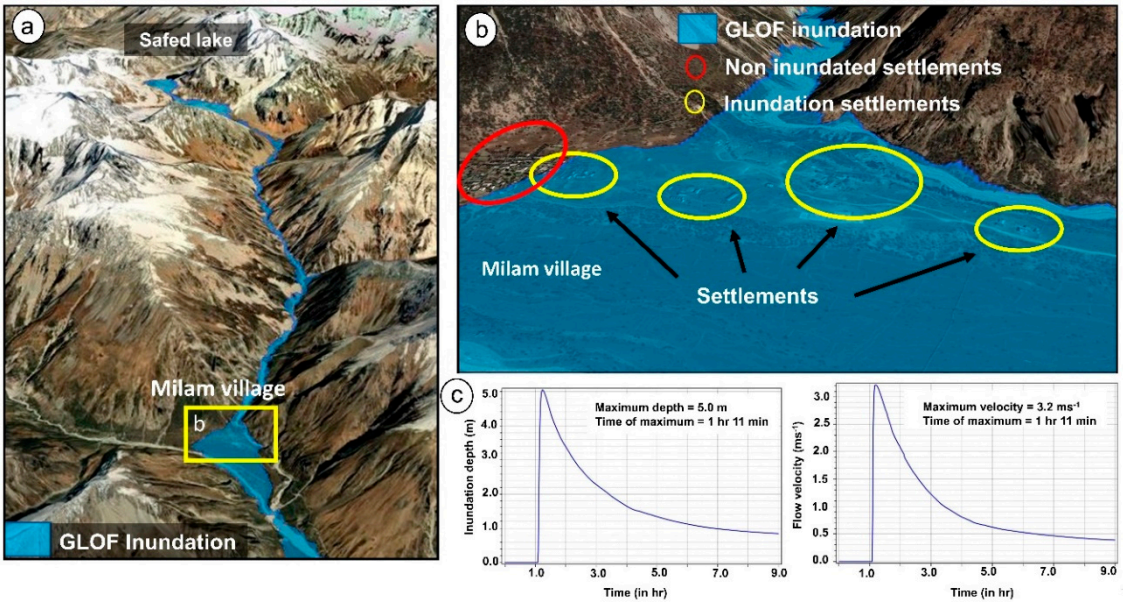

Figure 7. (**a**) GLOF inundation from Safed Lake to Milam village in a worst-case scenario (Scenario 1); (**b**) Milam village showing the inundated and non-inundated settlements; (**c**) plot showing the change of flow depth and velocity with time at Milam.

Table 2. The hydraulics of the GLOF hydrographs and the routed flow hydraulics at Milam village.

	Breach Hydrograph		At Milam		
GLOF Scenarios	**Peak Flood (m^3 s^{-1})**	**Time of Peak (min)**	**Maximum Inundation Depth (m)**	**Maximum Flow Velocity (m s^{-1})**	**Time of Maximum**
Scenerio-1	8181	6	5	3.2	1 h 15 min
Scenerio-2	5110	12	2.3	1.3	2 h 15 min
Scenerio-3	1495	22	0.9	0.3	6 h 35 min

4.3. Sensitivity Analysis

4.3.1. Model Sensitivity to Input Parameters

The sensitivity of the hydrodynamic model to breach width (B_w), time of failure (T_f) and Manning's N were evaluated by a series of hypothetical-scenario models. In order to assess the influence of one-dimensional breach parameters on the breach hydrograph, six hypothetical scenarios with varied B_w and T_f values were considered. At first, three scenarios were considered with varied T_f (30, 45 and 60 min) and a constant B_w (100 m). The peak discharge changes by ±11.5% when dT_f is 15 min. The time of peak discharge changes by ±4 to ±5 min when T_f is increased or decreased by 15 min (Figure 8a). Similarly, the remaining three scenarios were modeled by keeping T_f (30 min) constant and varying B_w (50, 75 and 100 m). The peak discharge decreased by 2.3% when B_w was reduced by 25 m. It further decreases by 14.4% when B_w was reduced by 50 m. The time of peak was delayed by 1 min and 4 min when B_w was reduced by 25 and 50 m respectively (Figure 8b). From the above GLOF scenario assessment, it is evident that GLOF hydrographs are more sensitive to the time of moraine failure compared to the width of the breach.

To evaluate the two-dimensional sensitivity of the model to the different boundary conditions (input breach hydrographs), the modeled hypothetical GLOF hydrographs with varied T_f were (Figure 8a) routed along the flow channel from the lake to Milam village. The inundation depth and flow velocity of the entire channel were evaluated. The maximum inundation depth decreases by 3.7% and 5.6% when T_f is increased by 15 and 30 min respectively. Similarly, the mean flow depth decreases by 2.9% and 5.4% when T_f is increased by 15 and 30 min respectively (Table 3). The evaluation of the maximum flow velocity along the given channel reveals a decrease of 2% and 3% when T_f is increased by 15 and 30 min respectively. Also, the mean velocity shows a decrease of 4% and 7.4% when T_f is increased by 15 and 30 min respectively (Table 3). The hydraulic properties of a GLOF at any point downstream is influenced by the initial breach hydrograph. The results show that the maximum inundation depth and the mean velocity are slightly more sensitive compared to the mean depth and maximum velocity respectively.

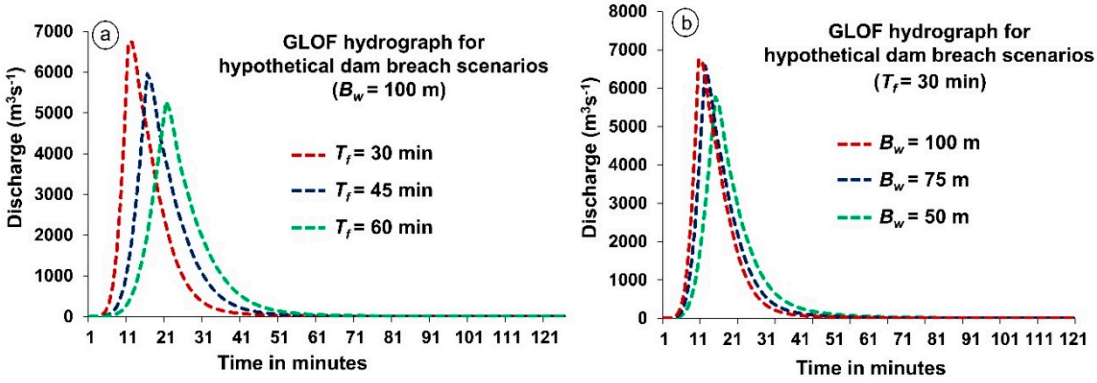

Figure 8. Breach hydrographs obtained for varied (**a**) time of moraine-failure (T_f) keeping breach width (B_w) constant; and (**b**) breach width (B_w) keeping the time of moraine-failure (T_f) constant.

Table 3. Hydraulic properties of potential GLOF along the flow channel for varied moraine-failure time.

Along Flow Channel				
	Inundation Depth		Flow Velocity	
Time of Failure (T_f)	Maximum	Mean	Maximum	Mean
0.5 h	15.8	4.02	19.8	3.24
0.75 h	15.2	3.90	19.4	3.11
1.0 h	14.9	3.80	19.2	3.00

At Milam village, maximum inundation depth decreases by 4.2% and 8.5% when T_f is increased by 15 and 30 min respectively. Likewise, the maximum flow velocity decreases by 4.3% and 7.5% when T_f is increased by 15 and 30 min respectively (Table 4). The temporal evaluation of the hydraulic parameters reveals a delay in the peak by 8 and 14 min when breach formation is increased by 15 and 30 min respectively. The timing of GLOF (peak) is sensitive to the initial flow hydrograph, which in turn is a function of the breach width (B_w) and the breach formation time (T_f). B_w and T_f are driven by various factors, such as the geometry and internal structure of the moraine dam and the type and magnitude of triggering events [44,45].

Table 4. Hydraulic properties of potential GLOF at Milam village for varied moraine-failure time.

At Milam Village			
Time of Failure (T_f)	**Maximum Depth (m)**	**Maximum Velocity (m s^{-1})**	**Time of Peak**
0.5 h	4.7	2.77	1 h 20 min
0.75 h	4.5	2.65	1 h 28 min
1.0 h	4.3	2.56	1 h 34 min

The sensitivity of the model to Manning's N was tested by performing a series of two-dimensional routing of the dam-breach hydrograph (see Figure 5). Keeping the dam-breach parameters constant (as in Section 4.2), two-dimensional routing was performed for varied Manning's N (0.03, 0.04, 0.05, 0.06 and 0.07). The results were evaluated by plotting the maximum and the mean flow depth and velocity against the Manning's roughness coefficient (Figure 9). The maximum flow velocity decreases with the increase in the channel roughness showing a correlation coefficient of 0.91 (strong correlation) (Figure 9a). Similarly, the mean velocity versus Manning's N revealed a similar trend with a correlation coefficient of 0.93 (strong correlation) (Figure 9b). The primary motive was to evaluate which parameter (flow velocity or flow depth) is more sensitive to the channel roughness.

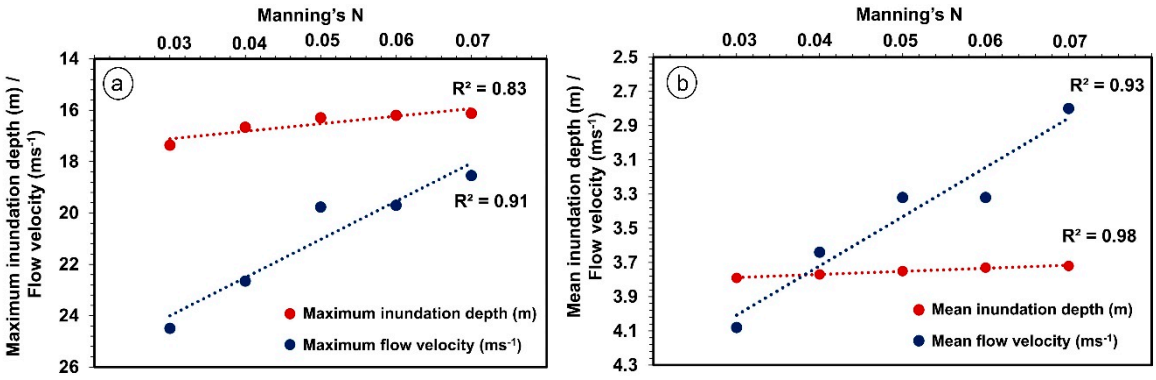

Figure 9. Plot of (**a**) Maximum inundation depth/flow velocity versus Manning's N; (**b**) mean inundation depth/flow velocity versus Manning's N.

The results reveal that flow velocity is more sensitive to the channel roughness compared to the inundation depth, as both maximum and mean depth do not show significant changes with change in the channel roughness. The Pearson correlation coefficient for maximum depth versus Manning's N was calculated to be 0.83 (strong correlation), and that of mean depth versus Manning's N was 0.98 (strong correlation). Figures 10 and 11 show the spatial distributions of the maximum depth and flow velocity from Safed Lake to Milam village for different Manning's roughness coefficients (N) along the channel.

4.3.2. Sensitivity to Channel Characteristics

This section of the study evaluates the sensitivity of the flow hydraulics (flow velocity and inundation depth) to channel characteristics (slope, top-width and terrain elevation). The slope calculated for every 100 m elevation contour was plotted against the mean velocity calculated for each elevation band. A similar analysis was performed by considering the mean depth and the slope of the channel. It is evident that the flow velocity linearly varies with change in the slope of the given channel with a correlation coefficient of 0.76 (Figure 12a). However, flow depth is independent (R^2 = 0.14) of the channel slope, as it shows a random variation (weak correlation) (Figure 12b).

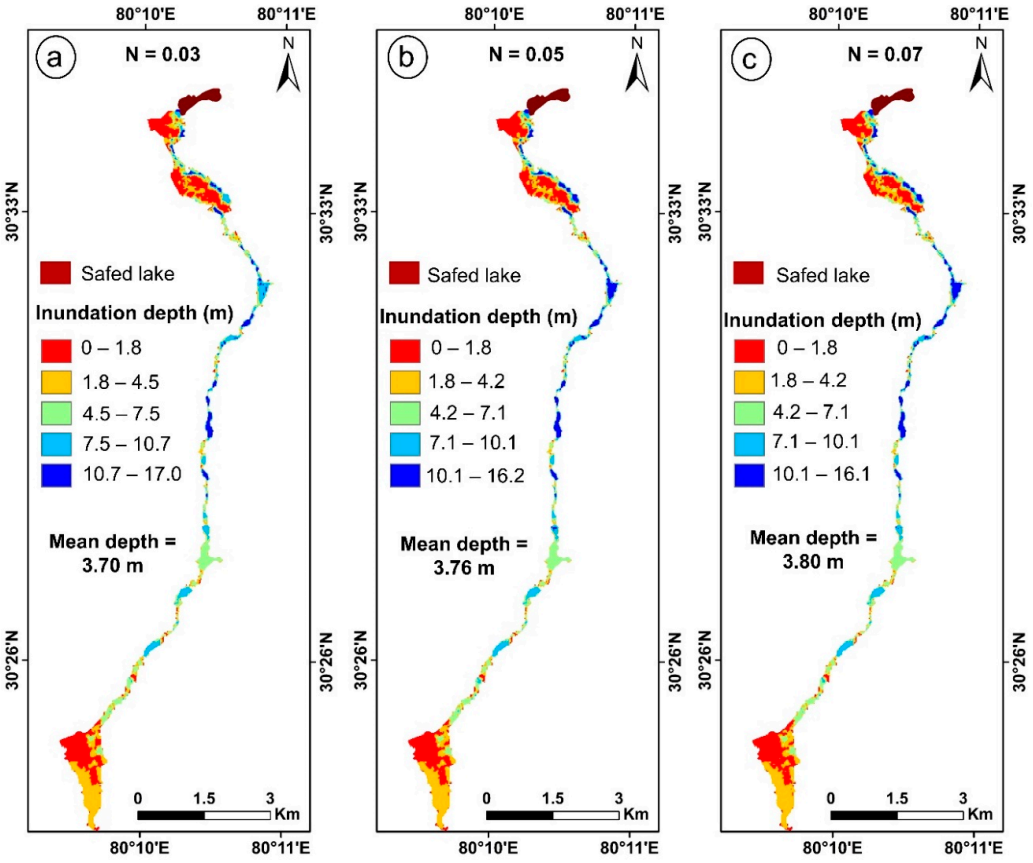

Figure 10. Spatial distribution of maximum inundation depth along the channel from Safed Lake to Milam village for varied Manning's N—(**a**) N = 0.03; (**b**) N = 0.05; (**c**) N = 0.07.

To evaluate the sensitivity of the hydraulic properties of a GLOF to the top-width of the flow channel, the flow velocity and depth are plotted against the top-width of the channel. The top-width was calculated along 20 cross-sections covering the entire flow channel, for which the mean flow depth and velocity were calculated. It is evident that the flow velocity and depth show similar trends when plotted against the respective top-width with correlation coefficients of 0.83 and 0.93 respectively (Figure 13). Both the flow velocity and depth tend to decrease as the top-width of the channel increases.

The sensitivity of GLOF hydraulics to terrain elevation (DEM) was evaluated by plotting the (SRTM DEM – ASTER DEM) elevation difference (in m) versus flow depth difference (in m) for every 250 m elevation contour band (see Section 3.3b) (Figure 14a). A correlation coefficient of 0.46 was calculated. Similarly, the plot of elevation difference (in m) versus flow velocity difference (in m/s) shows a correlation coefficient of 0.54 (Figure 14b). It is evident that GLOF hydraulics is sensitive to terrain elevation changes, with flow velocity being slightly more sensitive when compared to the flow depth. Both these coefficients show that there is a positive correlation between the elevation difference and flow depth difference and flow velocity difference, respectively. Practically, this reveals that the larger the difference between the DEMs used (3833–3583 m.a.s.l. elevation band in our case), the larger difference in modeled results (flow depth and flow velocity) observed among different DEMs.

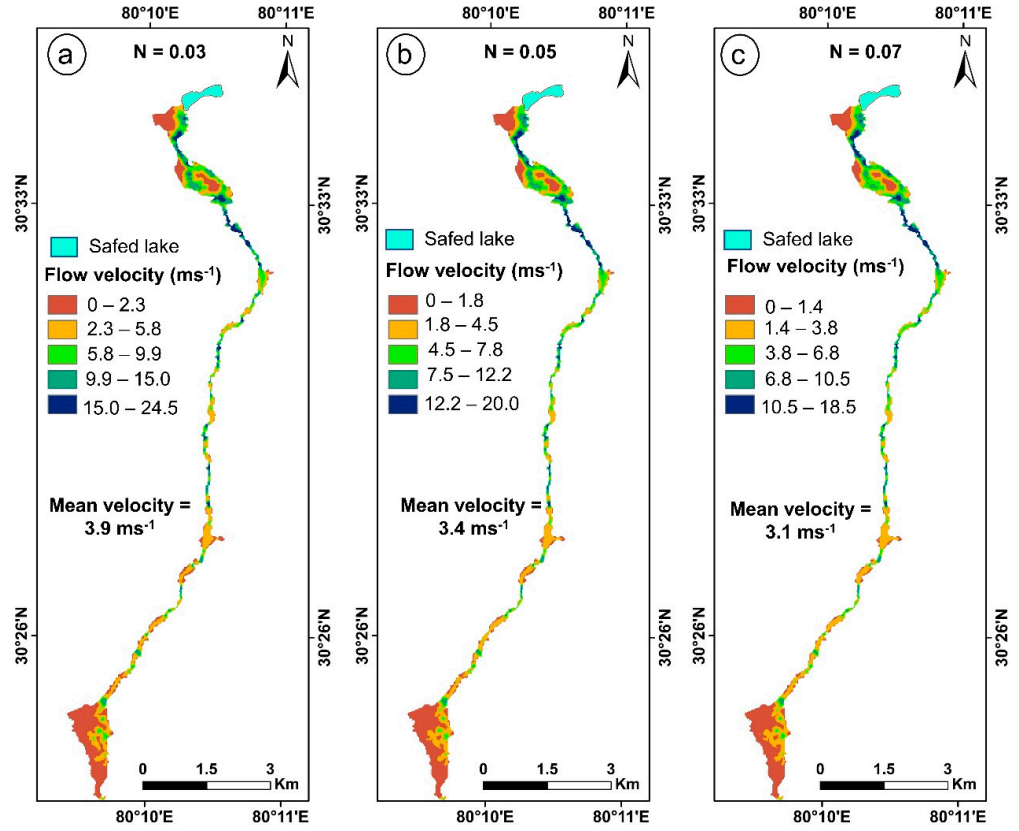

Figure 11. Spatial distribution of maximum flow velocity along the channel from Safed Lake to Milam village for varied Manning's N—(**a**) N = 0.03; (**b**) N = 0.05; (**c**) N = 0.07.

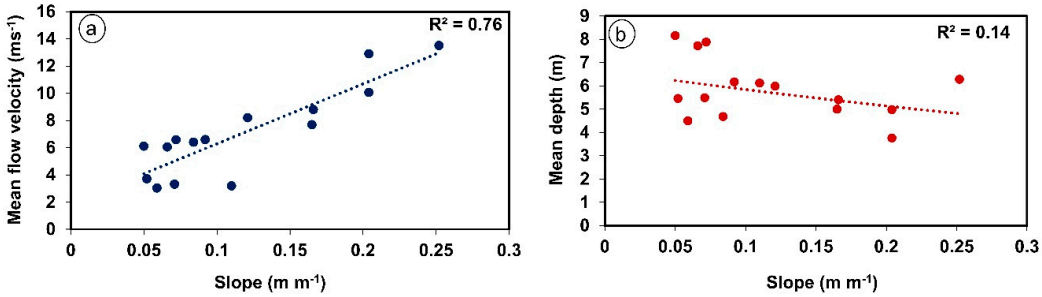

Figure 12. Plot showing (**a**) mean velocity versus slope of the channel; (**b**) mean depth versus slope of the channel; it is evident that the flow velocity linearly varies with the change in the slope of the given channel; flow depth is not dependent on the slope.

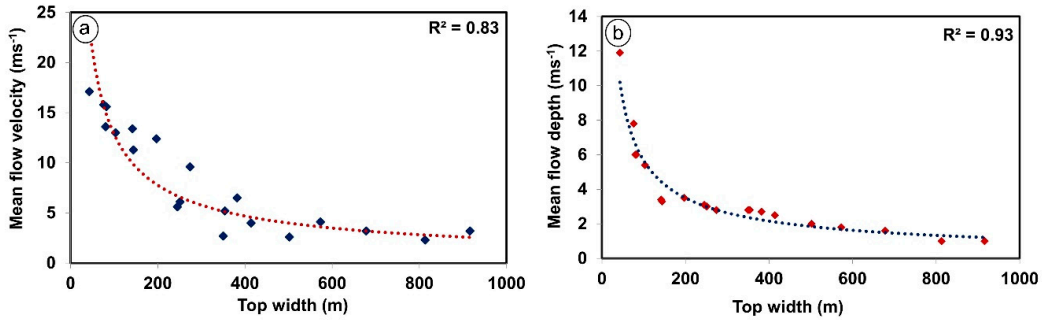

Figure 13. Plot showing (**a**) mean velocity versus top-width of the channel; (**b**) mean depth versus top-width of the channel; both flow velocity and flow depth vary similarly to the change in the top-width of the channel.

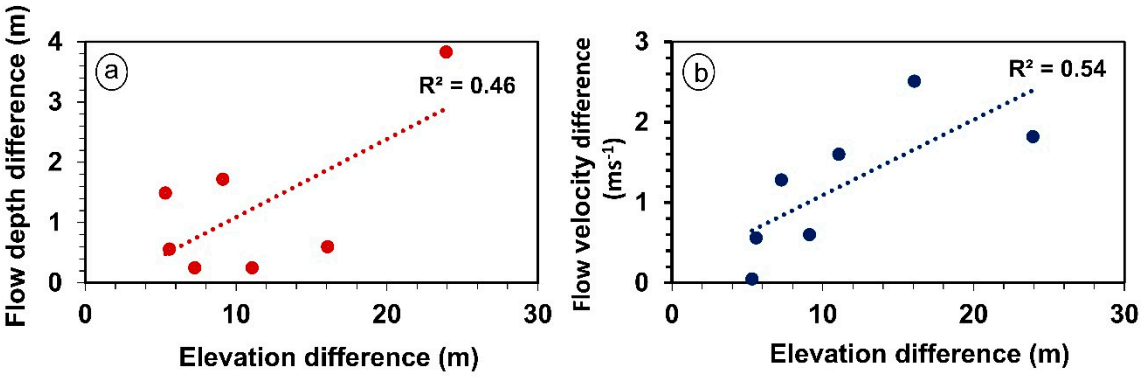

Figure 14. Each point data on either of the graphs is the average of the difference value (SRTM—ASTER) of terrain elevation (in m), flow depth (in m) and flow velocity (in m s^{-1}) for every 250 m elevation band along the flow channel (see Section 3.3b); (**a**) flow depth difference (m) versus terrain elevation difference (m); (**b**) flow velocity difference (m s^{-1}) versus terrain elevation difference (m).

5. Discussion

The study evaluated a series of potential GLOF scenarios of Safed Lake and their impact on the nearest settlement Milam village, using 1D and 2D dynamic modeling. The potential breach event in a worst-case GLOF scenario (h_b = 60 m) of Safed Lake produced a GLOF hydrograph with a peak discharge of 8181 m^3 s^{-1}. Hydrodynamic routing of the potential GLOF hydrograph along the given channel revealed inundation depth up to a maximum of 5 m and flow velocities up to 3.2 m s^{-1} at Milam village. The GLOF potentially inundates a part of the village, thereby affecting a total of 25 to 30 houses located at the site. The major part of the settlements in the village remains unaffected, as the flow channel takes a sharp turn towards the south and the flow is obstructed by the elevated terrain (see Figure 7b). Further, hazard assessments of the lake were carried out based on different breach depths (30 and 15 m). The maximum inundation depth at Milam village was reduced by 54% and 94% when h_b = 30 m and h_b = 15 m, respectively. Similarly, the flow velocity reduced by 59% and 90.6% when h_b = 30 m and h_b = 15 m respectively. In terms of hazard posed to Milam village, we further highlight the hazard of lateral erosion of the river banks, which may affect buildings not modeled to be flooded. This specific hazard also needs to be taken into consideration when designing flood protection and mitigation measured.

Hydrodynamic modeling of GLOFs involves a series of process-modeling, which includes dam breach formation and flood routing. A challenging task is to evaluate the accuracy of the modeled outputs, as physically-based hydraulic modeling is sensitive to the various inputs the model demands [46,47]. The process of moraine dam breach is complex and is dependent on many factors like height, width, and slope of the moraine [48–50]. The hydrograph obtained during a breaching process determines the flow hydraulics in the downstream region [47,50]. Moreover, the channel properties also affect GLOFs and their nature, by influencing the flow over a given terrain. The Manning's roughness coefficient has a significant effect on GLOFs, as it directly influences the peak discharge and flow velocity over a given channel [51–54]. Anacona et al. [50] performed a sensitivity analysis to evaluate the effect of Manning's N and breach hydrograph on GLOF. These parameters were reported to be the main controlling factors for a given GLOF event. Bajracharya et al. [51] stated the importance of Manning's N for accurate GLOF simulations. A 9% decrease in the peak discharge was observed as the Manning's N value was increased by 10% [14], whereas only 8% variation in the discharge was reported when Manning's N was varied by 30% [15]. This was attributed to the dominance of convective acceleration over bed-resistance, and the breach forming process too. Similar findings by Yochum et al. [54] suggest that hydraulic resistance is underestimated in high-gradient channels due to the dominance of flow acceleration on steep slopes. The sensitivity of the hydraulic models to simulate GLOF events varies from case to case depending upon the morphometric setting and input parameters.

It is therefore elementary to evaluate the sensitivity of these dynamic models and its simulated outputs to various hydraulic inputs and morphometric parameters.

Our study evaluated the sensitivity of the dynamic hydraulic model and its simulated outputs to various hydraulic inputs and morphometric parameters. For this, a series of hydrodynamic moraine-breach modeling and flood routing was performed to assess the sensitivity of flow hydraulics to different model input parameters and terrain characteristics. The sensitivity of the initial GLOF hydrograph to the total breach width (B_w) and breach formation time (T_f) was evaluated by considering six hypothetical moraine-breach scenarios with different combinations of B_w and T_f. It was evident that the GLOF hydrograph was more sensitive to the breach formation time (T_f) than the breach width (B_w). In order to evaluate the two-dimensional sensitivity of the model to the breach hydrographs, the modeled hypothetical GLOF hydrographs with varied T_f were (Figure 8a) routed along the flow channel from the lake to Milam village. The analysis revealed that the initial breach hydrograph determines the flow hydraulics of a routed GLOF. The hydraulic properties of a GLOF at any point downstream is sensitive to the initial breach hydrograph.

The relationships between the flow hydraulics (flow velocity and inundation depth) and channel characteristics were evaluated. The flow velocity is linearly dependent on the slope of the given flow channel. However, the flow depths do not show any relation with the slope of the channel and tend to vary in a random manner. In addition, the flow hydraulics were analyzed with respect to the top-width of the channel. Both flow velocity and inundation depth reveal a similar trend of decrease with an increase in the top-width of the channel. The choice of DEM is also crucial in the dynamic routing of GLOFs, as it affects flow hydraulics (both flow depth and velocity) (Figure 14).

6. Conclusions

The Himalaya hosts numerous glacial lakes and has experienced disastrous GLOFs in the past. Climate change-driven glacial retreat is the major reason behind the formation of such lakes. In this work, we analyzed the dynamics and evolution of Safed Lake (Uttarakhand, Central Himalaya), employed HEC-RAS to model several GLOF scenarios and evaluated the sensitivity of this model to changes in selected input parameters and DEMs used. Safed Lake is one of the largest glacial lakes, and underwent rapid glacier retreat-driven growth in past decades. We showed that the lake surface has grown from 0.10 km^2 (1968) to 0.23 km^2 (2018), and we estimated current lake volume to be 4.34×10^6 m^3, with the potential for future growth. The modeled flow hydraulics of a potential GLOF event revealed the part of Milam village, located 16.2 km downstream the lake, to be at great risk in a worst-case GLOF scenario, considering the dam incision till the base of the moraine (60 m breach depth), releasing the entire volume of the lake. However, the impact of a potential GLOF significantly reduces when the breach depth is reduced to half (30 m) and quarter (15 m). GLOF resulting from 15 m breach depth presents no risk of flooding to the village. Due to the fact the moraine of Safed Lake has a flat geometry, it is highly unlikely that the breach depth would reach its maximum. However, site-specific investigation and monitoring of the lake, moraine dam and its structure, and a detailed investigation of the magnitude of possible GLOF triggers, are highly recommended for advanced hazard and risk assessment. Further, steps for flood protection and water management can be implemented.

Author Contributions: Conceptualization, A.S., and A.E.; methodology, A.S., A.G., A.V.K., and A.E.; software, A.S.; validation, A.S., A.E., A.G. and A.V.K.; formal analysis, A.S. and A.G.; investigation, A.S. and A.E.; resources, A.S. and A.G.; data curation, A.S. and A.G.; writing—A.S. and A.E.; visualization, A.S.; supervision, A.G. and A.V.K.; project administration, A.G. and K.A.; funding acquisition, A.G. and A.V.K. All authors have read and agreed to the published version of the manuscript.

Funding: The research was funded by MHRD, MoES (project number IMPRINT 4096) and DST INSPIRE fellowship program.

Acknowledgments: The authors would like to acknowledge the Indian Institute of Technology, Roorkee, India for providing necessary infrastructure facilities. The authors would further like to acknowledge USGS, Digital Globe and NavInfo for the remote sensing datasets employed in the study. Adam Emmer was supported by the Ministry of Education, Youth and Sports of the Czech Republic within the National Sustainability Programme I (NPU I), grant number LO1415, and Supporting perspective human resources Programme of the Czech Academy of Sciences, project, "Dynamics and spatiotemporal patterns of glacial lakes evolution and their implications for risk management and adaptation in recently deglaciated areas".

Conflicts of Interest: The authors declare no conflict of interest.

References

1. Bolch, T.; Kulkarni, A.; Kääb, A.; Huggel, C.; Paul, F.; Cogley, J.G.; Frey, H.; Kargel, J.S.; Fujita, K.; Scheel, M.; et al. The state and fate of Himalayan glaciers. *Science* **2012**, *336*, 310–314. [CrossRef] [PubMed]
2. Nie, Y.; Sheng, Y.W.; Liu, Q.; Liu, L.S.; Zhang, Y.L.; Song, C.Q. A regional-scale assessment of Himalayan glacial lake changes using satellite observations from 1990 to 2015. *Remote Sens. Environ.* **2017**, *189*, 1–13. [CrossRef]
3. Richardson, S.D.; Reynods, J.M. An overview of glacial hazards in the Himalayas. *Quat. Int.* **2000**, *65*, 31–47. [CrossRef]
4. Veh, G.; Korup, O.; von Sprecht, S.; Roessner, S.; Walz, A. Unchanged frequency of moraine-dammed glacial lake outburst floods in the Himalaya. *Nature Clim. Chang.* **2019**, *9*, 379. [CrossRef]
5. Harrison, S.; Kargel, J.S.; Huggel, C.; Reynolds, J.; Shugar, D.H.; Betts, R.A.; Emmer, A.; Glasser, N.; Haritashya, U.K.; Klimeš, J.; et al. Climate change and the global pattern of moraine-dammed glacial lake outburst floods. *Cryosphere* **2018**, *12*, 1195–1209. [CrossRef]
6. Emmer, A. GLOFs in the WOS: Bibliometrics, geographies and global trends of research on glacial lake outburst floods (Web of Science, 1979–2016). *Natural Hazards Earth Syst. Sci.* **2018**, *18*, 813–827. [CrossRef]
7. Allen, S.K.; Rastner, P.; Arora, M.; Huggel, C.; Stoffel, M. Lake outburst and debris flow disaster at Kedarnath, June 2013: Hydrometeorological triggering and topographic predisposition. *Landslides* **2016**, *13*, 1479–1491. [CrossRef]
8. Carrivick, J.L.; Tweed, F.S. A global assessment of the societal impacts of glacier outburst floods. *Glob. Planet. Chang.* **2016**, *144*, 1–16. [CrossRef]
9. Worni, R.; Huggel, C.; Stoffel, M. Glacial lakes in the Indian Himalayas—From an area-wide glacial lake inventory to on-site and modeling based risk assessment of critical glacial lakes. *Sci. Total Environ.* **2013**, *468*, S71–S84. [CrossRef]
10. Allen, S.K.; Linsbauer, A.; Radhawa, S.S.; Huggel, C.; Rana, P.; Kumari, A. Glacial lake outburst flood risk in Himachal Pradesh, India: An integrative and anticipatory approach considering current and future threats. *Nat. Hazards* **2016**, *84*, 1741–1763. [CrossRef]
11. Raj, K.B.G.; Remya, S.N.; Kumar, K.V. Remote sensing-based hazard assessment of glacial lakes in Sikkim Himalaya. *Curr. Sci.* **2013**, *104*, 359–364.
12. Aggarwal, S.; Rai, S.; Thakur, P.K.; Emmer, A. Inventory and recently increasing GLOF susceptibility of glacial lakes in Sikkim, Eastern Himalaya. *Geomorphology* **2017**, *30*, 39–54. [CrossRef]
13. Shrestha, A.B.; Eriksson, M.; Mool, P.; Ghimire, P.; Mishra, B.; Khanal, N.R. Glacial lake outburst flood risk assessment of Sun Koshi basin, Nepal. *Geomat. Natural Hazards Risk* **2010**, *1*, 157–169. [CrossRef]
14. Jain, S.K.; Lohani, A.K.; Singh, R.D.; Chaudhary, A.; Thakural, L.N. Glacial lakes and glacial lake outburst flood in a Himalayan basin using remote sensing and GIS. *Natural Hazards* **2012**, *62*, 887–889. [CrossRef]
15. Mir, R.A.; Jain, S.K.; Lohani, A.K.; Saraf, A.K. Glacier recession and glacial lake outburst flood studies in Zanskar basin, western Himalaya. *J. Hydrol.* **2018**, *564*, 376–396. [CrossRef]
16. Sharma, R.K.; Pradhan, P.; Sharma, N.P.; Shrestha, D.G. Remote sensing and in situ-based assessment of rapidly growing South Lhonak glacial lake in eastern Himalaya, India. *Natural Hazards* **2018**, *93*, 393–409. [CrossRef]
17. Sattar, A.; Goswami, A.; Kulkarni, A.V. Hydrodynamic moraine-breach modeling and outburst flood routing—A hazard assessment of the South Lhonak lake, Sikkim. *Sci. Total Environ.* **2019**, *668*, 362–378. [CrossRef]
18. Emmer, A. *Glacial Hazards and Risks in Disaster Management Plans of Mountain States in India*; An Internal Report for the University of Zürich; The University of Zürich: Zürich, Switzerland, 2019; 11p.

19. Google Inc. *Google Earth Pro, v.7.1.5.1557*; Google Inc.: Menlo Park, CA, USA, 2015; Available online: https://earth.google.com/web/ (accessed on 30 September 2018).
20. Tachikawa, T.; Kaku, M.; Iwasaki, A.; Gesch, D.B.; Oimoen, M.J.; Zhang, Z.; Danielson, J.J.; Krieger, T.; Curtis, B.; Haase, J.; et al. *ASTER Global Digital Elevation Model Version 2-Summary of Validation Results*; NASA: Washington, DC, USA, 2011. Available online: https://pubs.er.usgs.gov/publication/70005960 (accessed on 1 February 2019).
21. Fujita, K.; Suzuki, R.; Nuimura, T.; Sakai, A. Performance of ASTER and SRTM DEMs, and their potential for assessing glacial lakes in the Lunana region, Bhutan Himalaya. *J. Glaciol.* **2008**, *54*, 220–228. [CrossRef]
22. Wang, W.; Yang, X.; Yao, T. Evaluation of ASTER GDEM and SRTM and their suitability in hydraulic modelling of a glacial lake outburst flood in southeast Tibet. *Hydrol. Process.* **2012**, *26*, 213–225. [CrossRef]
23. Sophie, B.; Pierre, D.; Eric, V.B. *GlobCOVER 2009 Products Description and Validation Report*; UCLouvain and ESA: Paris, France, 2010; Available online: http://due.esrin.esa.int/page_globcover.php (accessed on 1 February 2019).
24. Huggel, C.; Kääb, A.; Haeberli, W.; Teysseire, P.; Paul, F. Remote sensing based assessment of hazards from glacier lake outbursts: A case study in the Swiss Alps. *Can. Geotech. J.* **2002**, *39*, 316–330. [CrossRef]
25. Bolch, T.; Buchroithner, M.F.; Peters, J.; Baessler, M.; Bajracharya, S. Identification of glacier motion and potentially dangerous glacial lakes in the Mt. Everest region/Nepal using spaceborne imagery. *Natural Hazards Earth Syst. Sci.* **2008**, *8*, 1329–1340. [CrossRef]
26. Sattar, A.; Goswami, A.; Kulkarni, A.; Das, P. Glacier-Surface Velocity Derived Ice Volume and Retreat Assessment in the Dhauliganga Basin, Central Himalaya-A Remote Sensing and Modeling Based Approach. *Front. Earth Sci.* **2019**, *7*. [CrossRef]
27. Cook, S.J.; Quincey, D.J. Estimating the volume of Alpine glacial lakes. *Earth Surf. Dyn. Discuss.* **2015**, *3*, 559–575. [CrossRef]
28. Evans, S.G. The maximum discharge of outburst floods caused by the breaching of man-made and natural dams. *Can. Geotech. J.* **1986**, *23*, 385–387. [CrossRef]
29. Loriaux, T.; Casassa, G. Evolution of glacial lakes from the Northern Patagonia Icefield and terrestrial water storage in a sealevel rise context. *Glob. Planet. Chang.* **2013**, *102*, 33–40. [CrossRef]
30. O'Connor, J.E.; Hardison, J.H.; Costa, J.E. *Debris Flows from Failures of Neoglacial-Age Moraine Dams in the Three Sisters and Mount Jefferson Wilderness Areas, Oregon*; US Geological Survey Professional Paper; US Department of the Interior, US Geological Survey: Reston, VA, USA, 2001; Volume 1606, p. 93.
31. Yao, X.; Liu, S.; Sun, M.; Wei, J.; Guo, W. Volume calculation and analysis of the changes in moraine-dammed lakes in the north Himalaya: A case study of Longbasaba lake. *J. Glaciol.* **2012**, *58*, 753–760. [CrossRef]
32. Bolch, T.; Peters, J.; Yegorov, A.; Pradhan, B.; Buchroithner, M.; Blagoveshchensky, V. Identification of potentially dangerous glacial lakes in the northern Tien Shan. *Nat. Hazards* **2011**, *59*, 1691–1714. [CrossRef]
33. Byers, A.C.; McKinney, D.C.; Somos-Valenzuela, M.; Watanabe, T.; Lamsal, D. Glacial lakes of the Hinku and Hongu valleys, Makalu Barun National Park and Buffer Zone, Nepal. *Nat. Hazards* **2013**, *69*, 115–139. [CrossRef]
34. Che, T.; Xiao, L.; Liou, Y.A. Changes in glaciers and glacial lakes and the identification of dangerous glacial lakes in the Pumqu River Basin, Xizang (Tibet). *Adv. Meteorol.* **2014**, *2014*, 903709. [CrossRef]
35. Gruber, F.E.; Mergili, M. Regional-scale analysis of high-mountain multi-hazard and risk indicators in the Pamir (Tajikistan) with GRASS GIS. *Nat. Hazards Earth Syst. Sci.* **2013**, *13*, 2779–2796. [CrossRef]
36. Huggel, C.; Haeberli, W.; Kääb, A.; Bieri, D.; Richardson, S. An assessment procedure for glacial hazards in the Swiss Alps. *Can. Geotech. J.* **2004**, *41*, 1068–1083. [CrossRef]
37. Sattar, A.; Goswami, A.; Kulkarni, A.V. Application of 1D and 2D hydrodynamic modeling to study glacial lake outburst flood (GLOF) and its impact on a hydropower station in Central Himalaya. *Nat. Hazards* **2019**, *97*, 535–553. [CrossRef]
38. Froehlich, D.C. Peak ouTflow from breached embankment dam. *J. Water Resour. Plan. Manag.* **1995**, *121*, 90–97. [CrossRef]
39. Brunner, G.W. *HEC-RAS River Analysis System: User's Manual*; US Army Corps of Engineers, Institute for Water Resources, Hydrologic Engineering Center: Davis, User Manual, 2002; p. 320.
40. Klimeš, J.; Benešová, M.; Vilímek, V.; Bouška, P.; Rapre, A.C. The reconstruction of a glacial lake outburst flood using HEC-RAS and its significance for future hazard assessments: An example from Lake 513 in the Cordillera Blanca, Peru. *Nat. Hazards* **2014**, *71*, 1617–1638. [CrossRef]

41. Kougkoulos, I.; Cook, S.J.; Edwards, L.A.; Clarke, L.J.; Symeonakis, E.; Dortch, J.M.; Nesbitt, K. Modelling glacial lake outburst flood impacts in the Bolivian Andes. *Nat. Hazards* **2018**, *94*, 1415–1438. [CrossRef]
42. Wang, W.C.; Gao, Y.; Anacona, P.I.; Lei, Y.B.; Xiang, Y.; Zhang, G.Q.; Li, S.H.; Lu, A.X. Integrated hazard assessment of Cirenmaco glacial lake in Zhangzangbo valley, Central Himalayas. *Geomorphology* **2018**, *306*, 292–305. [CrossRef]
43. Brunner, G.W. *HEC-RAS River Analysis System 2D Modeling User's Manual*; US Army Corps of Engineers—Hydrologic Engineering Center: Davis, User Manual, 2016; pp. 1–171.
44. Clague, J.J.; Evans, S.G. A review of catastrophic drainage of moraine–dammed lakes in British Columbia. *Quat. Sci. Rev.* **2000**, *19*, 1763–1783. [CrossRef]
45. Emmer, A. Geomorphologically effective floods from moraine-dammed lakes in the Cordillera Blanca, Peru. *Quat. Sci. Rev.* **2017**, *177*, 220–234. [CrossRef]
46. Anacona, P.I.; Norton, K.P.; Mackintosh, A. Moraine-dammed lake failures in Patagonia and assessment of outburst susceptibility in the Baker Basin. *Nat. Hazards Earth Syst. Sci.* **2014**, *14*, 3243. [CrossRef]
47. Westoby, M.J.; Glasser, N.F.; Brasington, J.; Hambrey, M.J.; Quincey, D.J.; Reynolds, J.M. Modelling outburst floods from moraine-dammed glacial lakes. *Earth-Sci. Rev.* **2014**, *134*, 137–159. [CrossRef]
48. Pickert, G.; Weitbrecht, V.; Bieberstein, A. Breaching of overtopped river embankments controlled by apparent cohesion. *J. Hydraul. Res.* **2011**, *49*, 143–156. [CrossRef]
49. Wang, X.; Liu, S.; Guo, W.; Xu, J. Assessment and simulation of glacier lake outburst floods for Longbasaba and Pida lakes, China. *Mt. Res. Dev.* **2008**, *28*, 310–317.
50. Anacona, P.I.; Mackintosh, A.; Norton, K. Reconstruction of a glacial lake outburst flood (GLOF) in the Engaño Valley, Chilean Patagonia: Lessons for GLOF risk management. *Sci. Total Environ.* **2015**, *527*, 1–11. [CrossRef] [PubMed]
51. Bajracharya, S.R.; Mool, P.K.; Shrestha, B.R. *Impact of Climate Change on Himalayan Glaciers and Glacial Lakes: Case Studies on GLOF and Associated Hazards in Nepal and Bhutan*; ICIMOD Publication 169; International Centre for Integrated Mountain Development and United Nations Environmental Programme Regional Office Asia: Patan, Nepal, 2007.
52. Carrivick, L.J. Application of 2D hydrodynamic modeling to high-magnitude outburst floods: An example from Kverkfjöll, Iceland. *J. Hydrol.* **2006**, *321*, 187–199. [CrossRef]
53. Carling, P.; Villanueva, I.; Herget, J.; Wright, N.; Borodavko, P.; Morvan, H. Unsteady 1D and 2D hydraulic models with ice dam break for Quaternary megaflood, Altai Mountains, southern Siberia. *Glob. Planet. Chang.* **2010**, *70*, 24–34. [CrossRef]
54. Yochum, S.E.; Bledsoe, B.P.; David, G.C.L.; Wohl, E. Velocity prediction in high-gradient channels. *J. Hydrol.* **2012**, *424–425*, 84–98. [CrossRef]